3D-macroporous chitosan-based scaffolds with *in situ* formed Pd and Pt nanoparticles for nitrophenol reduction

Dmitriy Berillo [1,2] * *and Andrew Cundy*[3]

[1]School of Pharmacy and Biomolecular Sciences, University of Brighton, Brighton, UK

[2]Department of Biotechnology, Center for chemistry and chemical engineering, Lund University, P.O. Box 124, 22 100, Lund, Sweden.

[3]School of Ocean and Earth Science, University of Southampton, National Oceanography Centre (Southampton),UK.

* Corresponding author: Dmitriy Berillo School of Pharmacy and Biomolecular Sciences, University of, Brighton, Brighton, UK, e-mail: D.Berillo@brighton.ac.uk

Tel: +44 (0)1273642015

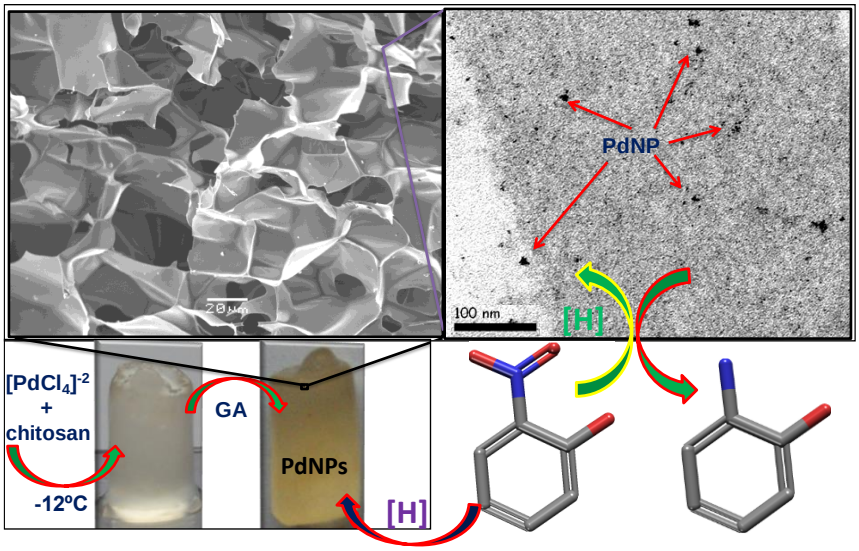

Published as a research article in:

***Carbohydrate Polymers* 192 (2018) pp 166-175**

3D-macroporous chitosan-based scaffolds with *in situ* formed Pd and Pt nanoparticles for nitrophenol reduction

*Dmitriy Berillo [1,2] * and Andrew Cundy[3]*

[1]School of Pharmacy and Biomolecular Sciences, University of Brighton, Brighton, UK

[2]Department of Biotechnology, Center for chemistry and chemical engineering, Lund University, P.O. Box 124, 22 100, Lund, Sweden.

[3]School of Ocean and Earth Science, University of Southampton, National Oceanography Centre (Southampton), UK.

* Corresponding author: Dmitriy Berillo School of Pharmacy and Biomolecular Sciences, University of Brighton, Brighton, UK, e-mail: D.Berillo@brighton.ac.uk

Phone: +44 (0)1273642015

Abstract

3D-macroporous chitosan-based scaffolds (cryogels) were produced via growth of metal-polymer coordinated complexes and electrostatic interactions between oppositely charged groups of chitosan and metal ions under subzero temperatures. A mechanism of reduction of noble metal complexes inside the cryogel walls by glutaraldehyde is proposed, which produces discrete and dispersed noble metal nanoparticles. 3D-macroporous scaffolds prepared under different conditions were characterised using TGA, FTIR, nitrogen adsorption, SEM, EDX and TEM, and the distribution of platinum nanoparticles (PtNPs) and palladium nanoparticles (PdNPs) in the material assessed. The catalytic activity of the *in situ* synthesised PdNPs, at 2.6, 12.5 and 21.0 μg total mass, respectively, was studied utilising a model system of 4-nitrophenol reduction. The kinetics of the reaction under different conditions (temperature, concentration of catalyst) were examined, and a decrease of catalytic activity was not observed over 17 treatment cycles. Increasing the temperature of the catalytic reaction from 10 to 22 and 35 °C by PdNPs supported within the cryogel increased the kinetic rate by 44 and 126%, respectively. Turnover number and turnover frequency of the PdNPs catalysts at room temperature were in the range 0.20 - 0.53 h^{-1}. The conversion degree of 4-nitrophenol at room temperature reached 98.9% (21.0 μg PdNPs). Significantly less mass of palladium nanoparticles (by 30-40 times) was needed compared to published data to obtain comparable rates of reduction of 4-nitrophenol.

Keywords: macroporous cryogels, chitosan, palladium nanoparticles, platinum nanoparticles, nitrophenol, catalysis.

1. Introduction

The last few decades have seen a growing interest in the application of chitosan (CS) as an industrial polymer (Guibal, 2005; Laudenslager, Schiffman, & Schauer, 2008; Qu, Wirsén, & Albertsson, 1999; Qu, Wirsén, Olander, & Albertsson, 2001). CS is a product of deacetylation of the natural (and renewable) polymer chitin, the second most common natural polysaccharide after cellulose (Berger et al., 2004; Kasaai, 2010), and consists of copolymers of D-glucosamine with N-acetyl-D-glucosamine. CS can show diverse properties (Brack, Tirmizi, & Risen, 1997; Laudenslager et al., 2008; Qu et al., 1999; Qu et al., 2001), and has been applied in a range of recent studies as a natural or "green" biopolymer for food technology, biotechnology, medicinal and environmental (e.g. water clean-up) applications(Ali, El-Aty, Badawy, & Ali, 2018; Bertoni, González, García, Sala, & Bellú, 2018; Hataf, Ghadir, & Ranjbar, 2018; Hu et al., 2018; Zahir-Jouzdani et al., 2018). CS and its derivatives with imidazole or dihydronicotinamide moieties and other modifications have also shown organocatalytic activity (El Kadib, 2015; Mahé, Brière, & Dez, 2015). CS shows a strong tendency to interact with polyphosphate, citrate, and metal ions, in particular with transition metals, and has also been extensively utilised for metal nanoparticle stabilisation (Berger et al., 2004; Berillo, Mattiasson, & Kirsebom, 2014; Guibal, 2005; Laudenslager et al., 2008; Yang et al., 2012). Metal-polymer coordinated complex formation is strongly dependant on the number of free amino groups and the hydrophilicity of the adsorbent structure (Kurita, 2006). The fundamental mechanism of adsorption of negatively charged metal complexes by chitosan is via donor-acceptor interactions between free electron pairs doublets of chitosan's amine functionality with vacant orbital positions of the metal (Berillo et al., 2014; Guibal, 2005; Kramareva et al., 2004; Wu & Jin, 2010) . The electrostatic interaction plays a primary function in the sorption process (Draget, Värum, Moen, Gynnild, & Smidsrød, 1992) and is strongly influenced by the degree of protonation of the amine groups. This increases with a decrease in pH, hence the electrostatic attraction between negatively charged metal complexes and the positively charged amine groups increases at lower pH (Berillo et al., 2014; Brack et al., 1997;

Guibal, Sweeney, Vincent, & Tobin, 2002). Aqueous CS solutions under mildly acidic conditions are therefore attractive as a feedstock for creating composite materials containing metal nanoparticles (NPs) (Berillo et al., 2014; Boufi, Vilar, Ferraria, & do Rego, 2013; Corma & Garcia, 2008; Yang et al., 2012), including macroporous spheres and hydrogels.

It is well known that in order to produce 3D-macroporous hydrogels, use of a cross linking agent is necessary (Berillo & Volkova, 2014; Dainiak et al., 2010; Gun'ko, Savina, & Mikhalovsky, 2013; Kirsebom et al., 2013; V. I. Lozinsky, Plieva, Galaev, & Mattiasson, 2001; Savina, Ingavle, Cundy, & Mikhalovsky, 2016). In most cases chemical cross-linking agents with double or more active functionalities (aldehyde, carboxylic, isocyanate, isothiocyanate, etc.), or enzymes, are used as cross-linkers in the production of hydrogels (Guibal et al., 2002; Qu et al., 1999) and cryogels (Berillo & Volkova, 2014; Dainiak et al., 2010; Kirsebom et al., 2013; V. Lozinsky, Zubov, Kulakova, Titova, & Rogozhin, 1992). There are a few examples of hydrogel or cryogel preparation with incorporated nanoparticles (NPs), for instance, via the three step preparation of macroporous scaffolds with incorporated AgNPs, which includes preparation of the scaffold, subsequent treatment with silver salt and reduction by borohydride,(Loo, Krantz, Fane, Hu, & Lim, 2015). A disadvantage of this approach however is the sometimes uneven distribution of the formed NPs within the material. A two-step approach has also been proposed, which includes the preparation of a nanoparticles suspension and its copolymerisation under cryo-conditions, which also has significant drawbacks including the difficulty of handling of NPs, probable blocking of the active sites of NPs and decrease of activity (Loo et al., 2015).

In the present study, we demonstrate a novel, reproducible and facile two step preparation procedure for chitosan-based macroporous hydrogels with *in situ* formed well distributed Pt or Pd nanoparticles.

Recently, the potential utility of highly-dispersed immobilised (i.e. supported) PdNPs and PtNPs for various applications in catalysis and sensor materials has been demonstrated (Emin, Gu, Remigy, & Lahitte, 2015; Komathi, Palaniappan, Manisankar, Gopalan, & Lee, 2010; Li et al., 2013; Liu, Ruiz, & Astruc, 2017; Murugan & Vimala, 2013; Sachse et al., 2011; Venkatesham,

Ayodhya, & Veerabhadram, 2015; Vilian et al., 2017). Regarding the support material for the catalyst, key requirements which must be taken into account are thermal and chemical stability during the reaction process, and a useable/flexible geometrical structure (Wu & Jin, 2010). Here, we examine the mechanical properties and stability of chitosan-based cryogels, and the characteristics of their incorporated noble metal nanoparticles (using TGA, FTIR, SEM, EDX and TEM), propose a reduction mechanism for the *in-situ* production of stabilised dispersed Pt and PdNPs, and assess their catalytic activity using synthesised monolithic flow-through PdNP-bearing reactors on a model system of 4-nitrophenol (4NP).

Materials

Sodium tetrachloropalladate $Na_2[PdCl_4]$ was from Aldrich Chem.Co (Milw. WI USA). Potassium tetrabromoplatinate $K_2[PtBr_4]$ and sodium tetrachloroplatinate $Na_2[PtCl_4]$ were synthesised by known methods (Bronstein et al., 1998) involving dissolution from platinum (II) bromide β-$PtBr_2$ and platinum (II) chloride β-$PtCl_2$ respectively, which were provided by Engelhard industries (Stockholm). Medium viscosity chitosan with 85% degree of acetylation and 50% (v/v) glutaraldehyde solution were from Aldrich (Steinheim, Germany), sodium borohydride 98% and 4-nitrophenol were from Fluka (Steinheim, Germany). Sodium acetate trihydrate was provided by Merck (Germany).

2. Methods

2.1 Preparation of cryogels with *in situ* reductive formation of platinum and palladium nanoparticles (PtNPs, PdNPs)

Chitosan (CS) was dissolved in different concentrations of aqueous acetic acid (33-200 mM), to a set volume of 1.1 % (w/v) CS. 14.5mM of $Na_2[PdCl_4]$ or $K_2[PtBr_4]$ or $Na_2[PtCl_4]$ (0.07 - 0.28 mL) was added to the polymer and vigorously mixed. The mixed solutions with final concentrations of chitosan of 1 % and $Na_2[PdCl_4]$ of 0.05, 0.2, 0.4 or 0.8 mM (and volume of 0.5mL) were rapidly transferred into a glass tube (diameter 7 mm) and frozen at -12 ºC in a cooled liquid cryostat. After

being frozen over 24 h the samples were thawed at room temperature and washed with water. The free palladium and platinum complex content in the wash solution was estimated using ICP MS analysis, which did not show the presence of the target ions.

Cryogels containing $[PdCl_4]^{2-}$ with concentrations of 0.05, 0.2 or 0.4 mM (or $[PtCl_4]^{2-}$ with concentrations of 1.0, 2.0 or 4.0 mM) were placed into a 2.5 % (v/v) glutaraldehyde (GA) solution in 0.1 M phosphate buffer (pH 7.4). The cryogels were incubated at room temperature overnight in a stationary mode to reduce the metal complexes into their corresponding metal NPs, and also to chemically cross-link the CS, over which time the colour of samples changed from white to yellow indicating the formation of Schiff's base groups. Then samples were removed from the solution and extensively washed with water (20 mL x 3 times). Solutions were filtered through a 0.22 μm membrane and analysed for Pd and Pt content using ICP-MS in order to prove that neither NPs nor metal complexes were leaking out of the scaffold, and to estimate the yield of metal complex binding. The cryogels with *in situ* formed nanoparticles were stored in a refrigerator until further use.

2.2 In situ reductive formation of PdNPs in acetonitrile-amended cryogel

In order to produce a uniform cryogel it was necessary to slow down the gel formation process, therefore a 14.5 mM solution of $Na_2[PdCl_4]$ (0.087 mL) was mixed with 0.05 mL acetonitrile (ACN) and 0.0777mL water. Then, the solution was mixed with 1.363 mL of 1.1% (wt/v) chitosan solution, and rapidly frozen at -12 ºC. After being frozen over 24 h at -12 ºC the $[PdCl_x(ACN)_y(NH_2\text{-}CS)_z]^{2-}$ cryogels were transferred into a 2.5% (v/v) GA solution in 0.1 M phosphate buffer (pH 7.4). The cryogels were incubated at room temperature for 3 h and then extensively washed with water. For long term storage cryogels can be stored in alcohol solution or freeze dried and stored at room temperature.

2.3 Cryogels characterisation.

Transmission electron microscopy (TEM) was used to analyse the obtained cryogels. A thin slice of the cryogel was arranged on a copper grid and the specimen was stained using a 1 % uranyl acetate solution for 60 seconds, after which the excess liquid was removed and the sample dried (Supplementary information).

2.4 Catalytic activity of chitosan-based cryogels containing PdNPs

The catalytic activity of cryogels containing different quantities of PdNPs (0.05, 0.2 and 0.4 mM) was studied in batch mode at room temperature (22 ºC). A cryogel with volume 0.5 mL was placed into 7 mL 50 mM carbonate buffer at pH 10 where 0.15 mL of 50 mM stock solution of 4-nitrophenol(4NP) in ethanol was added. Then, 0.15 mL of 0.2 M freshly dissolved $NaBH_4$ in carbonate buffer was added under gentle magnetic stirring. A reaction mixture containing 5 mM 4NP and $NaBH_4$ solution (2 mM) was continuously recirculated through a flow quartz cuvette at a flow rate of 0.5 mL/min and the absorbance measured at 400 nm in automatic mode every minute using a UV-vis (Biowave II) spectrophotometer. All experiments for each concentration of PdNPs were performed in duplicate, and indicated as sample a & b. For further testing of the catalytic activity the cryogel (without preliminary washing) was immersed into a fresh solution of 4NP. Cryogels were kept in carbonate buffer solution at 4 ºC overnight between experiments. Every catalytic cycle of reduction of 4NP took at least 2 h. The experiments were performed at different temperatures using a thermostat (Lauda), which was set for 10 and 35 ºC, respectively.

A control experiment was performed in batch mode at room temperature (22 ºC). A 0.15 mL volume of stock solution of 4-nitrophenol(4NP) (0.05 mM) was diluted in 50 mM carbonate buffer at pH 10 to 6.85 mL and then 0.15 mL of 0.1 M $NaBH_4$ was added. The solution was continuously recirculated through the blank CS-GA cryogel without PdNPs at a flow rate of 0.5 mL/min via a quartz cuvette where absorbance measurements were performed at 400 nm in automatic mode every minute.

The lifetime of the catalyst was expressed using the turnover number (TON), which is the number of moles of substrate that a mole of the catalyst can convert before inactivation (Hagen, 2015). The TON was calculated according to equation 1.

$$TON = [4NP] * [MeNPs]^{-1} * t \quad \text{Eq.1}$$

(where [4NP] and [MeNPs] are the molar concentrations of the substrate and the catalyst, and t is the overall catalytic time) and the turnover frequency (TOF) was calculated using equation 2.

$$TOF = [4NP] * [conversion]*[MeNPs]^{-1} * t^{-1} \quad \text{Eq.2}$$

Further methods used for characterization of cryogels (FTIR, ionic chromatography, SEM, rheology, swelling degree) are described in detail in Supplementary Information.

3. Results and Discussion

3.1 Preparation of cryogels with *in situ* formed Pd and Pt nanoparticles

For the formation of cryogels, it is critical that freezing of the solvent takes place prior to the cross-linking reaction (Kirsebom et al., 2013). Rapid mixing, cooling and freezing of reaction mixtures of CS and $Na_2[PdCl_4]$ or $Na_2[PtCl_4]$ down to -12 °C allowed crystallisation of the solvent and phase separation, with the liquid phase containing a concentrated solution of dissolved solutes such as CS, acetic acid (HAc), noble metal complexes and bound non-frozen water, which solvates the solutes. The solid phase was formed of pure ice crystals, which act as a porogen (Gun'ko et al., 2013; Kirsebom et al., 2013; V. I. Lozinsky et al., 2003) to create a macroporous structure. Under semi-frozen conditions in the liquid phase, the macrochains of CS were chelated by the noble metal complexes not due to low temperature, but due to a cryoconcentration effect, resulting in the formation of a stable 3D-network. After chelation reached equilibrium, the sample was thawed and the ice crystals melted, following which the polymeric network maintained its shape, i.e. the macroporous structure where the ice crystals were present earlier (Berillo et al., 2014).

The development of a coordinated bond between the non-protonated amino groups of CS and the noble metal complexes was responsible for the gelation process.

The increase in viscosity over a 30 minute period (at standard temperature) for a CS solution containing 0.2 mM $[PdCl_4]^{2-}$ (Figure S1) was significantly more rapid than that of the same solution in the presence of ACN. This observation indicates that the ligand exchange process for the $[Pd(ACN)_2Cl_2]^{-2}$ complex with CS occurred more slowly than that of tetrachloropalladate. Taking into account these data it can be concluded that cryogel formation took place after solvent crystallization, which took place within 5 min of mixing of the reagents. The change of viscosity for a solution containing 0.4 mM of $[PdCl_4]^{2-}$ indicated that the hydrogel formation or cross-linking process was completed within 20-30 minutes at standard conditions (Figure S1). The viscosity of CS solution with 0.05 mM and 0.2 mM of $[PdCl_4]^{2-}$ did not reach an equilibrium, indicating the concentration dependence of the process.

Therefore by utilizing a complex of $[Pd(ACN)_2Cl_2]^{-2}$ it is possible to prepare a macroporous catalyst with higher noble metal content, via delaying hydrogel formation, which allows freezing of the solution prior to gelation.

ICP-MS analysis of wash water from freeze dried cryogels containing Pd complexes did not reveal any free Pd ions in the solution, confirming the stable binding of Pd complexes with the cryogel scaffold. Non freeze-dried, freshly prepared, cryogels showed a yield of 99.66% of the Pd-CS complex (concentration of palladium of 1-2μg/L). Additionally, analysis of the phosphate buffer with glutaraldehyde did not reveal any palladium ions in solution after the (glutaraldehyde) reduction & cross-linking process (discussed below).

Cryogels were characterised by a semi-translucent structure, most probably due to the generation of relatively thicker pore walls compared to ordinary cryogels (Figure 1) (Kirsebom et al. 2013). This structure may be attributed to the hydrophilic nature of the polymer, the relatively low degree of cross-linking, and an absence of phase separation. This observation is in agreement with previous studies where semi-transparent cryogels based on hyaluronic acid were reported (Kirsebom et al., 2013; Oelschlaeger, Bossler, & Willenbacher, 2016).

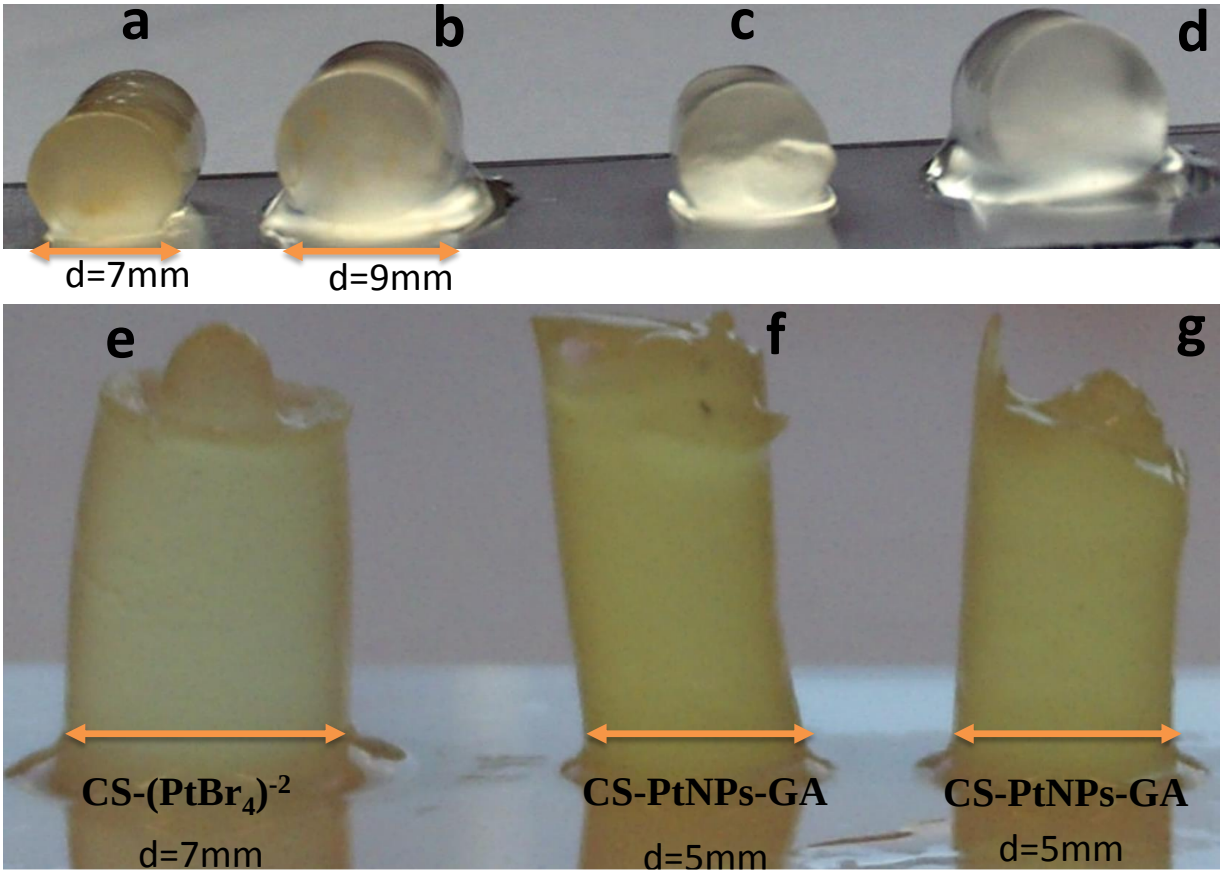

Figure 1. Photographs of cryogels of : CS-$[PtBr_4]^{-2}$ 4 mM (a, b) and 2 mM (c, d) (before swelling in water (a, c)), after swelling in water and reaching equilibrium (b, d); e) freshly prepared CS-$[PtBr_4]^{-2}$ 4 mM and after treatment with GA: (f) CS-PtNPs-GA 2 mM, (g) CS-PtNPs-GA 4 mM.

It was visually observed that cryogels containing palladium or platinum were not light sensitive, in contrast to cryogels containing gold complexes (Berillo et al., 2014), which may relate to the formation of the stable coordination bonds Pd-O and Pd-N. Also, there is a significant difference in standard electrode potentials between gold and platinum or palladium systems, i.e. standard electrode potentials for complexes of platinum and palladium E^o ($[PtCl_4]^{2-}$/Pt,4Cl^-) +0.73 V and E^o ($[PdCl_4]^{2-}$/Pd,4Cl^-) +0.62 V, respectively (Adlim, Abu Bakar, Liew, & Ismail, 2004). These potentials are lower than those for gold complexes (of $E_0[AuCl_4]^-$ / Au^0 0.93 V), whose ionic cryogels show a tendency to degrade in the presence of light, and produce AuNPs suspensions (Berillo et al., 2014). Pt and Pd-bearing components have less oxidative ability compared to gold

complexes, therefore most probably the energy of visible light is not enough for activation of a simultaneous reduction process and as a consequence the material is stable under visible light.

To prepare cryogels containing *in-situ* synthesized Pt or Pd nanoparticles, while avoiding dissolution or damage of the cryogel under acidic conditions, the cryogels were treated with GA. As a control experiment the cryogels were reduced by borohydride, which however resulted in collapse of the cryogel structure. Treatment with GA led to a condensation reaction of the primary amino groups of CS with aldehyde groups resulting in formation of Schiff's bases, i.e. cross-linking of CS (Berger et al., 2004) (Shi, Zhang, Shen, Bi, & Dai, 2013). Concurrently, the presence of aldehyde functionality and noble metal complexes triggers a simultaneous oxidation-reduction process. The oxidation of aldehyde to carboxylic groups (E^0 [HC=O]/[COOH] = -0.58 V) by noble metal complexes leads to reduction to the zero valent state, forming Pt or Pd nanoparticles (reaction 2 below), respectively. To confirm the reductive properties of GA a number of control experiments of GA with tetrachloropalladate were performed. The mixture of tetrachloropalladate with GA did not change colour over time, confirming that the reaction did not take place in acidic conditions, which shifted the equilibrium of the reaction to the reduction process. The reaction performed in carbonate buffer (pH 7.2-7.6) resulted in CO_2 emission and formation of PdNPs precipitates. H^1-NMR spectra of the reaction mixture at different conditions were recorded, which did not show significant changes, probably due to the formed glutaric acid instantly acting as a stabilising agent for PdNPs. It is well known that di and tricarbonic acids can act as a stabilising agent, the most famous example of which is the preparation of noble metal nanoparticles using citric acid.(Maritz & van Eldik, 1976)

The driving force of the simultaneous reduction process is the difference in standard redox potentials between oxidant and reductant, whereby the larger the change of standard redox potential the faster the reaction that takes place. Previously, the possibility of reduction of Pt using formaldehyde has been observed, however, the mechanism of formation of nanoparticles and their subsequent stabilisation was not shown. A possible mechanism for the reduction reaction of noble metal-polymer coordinated complexes by GA is shown below (reaction 1).

$[MeCl_{4-n}Lg_n]^{2-} + H(O=)C(CH_2)_3CH(=O) + H_2O \Rightarrow [Me^0Lg_{n-x}] + (4-n)Cl^- + xLg + 2H^+ +$

$+ HOOC(CH_2)_3COOH$ **reaction 1**

where Lg = ligand (-R-NH_2 or R-OH, Ac^-), and Me = Pt or Pd, $0<n\leq4$ and $x\leq n$

The resulting zero valent noble metal nanoparticles are stabilised by various ligands from the polymer, which have been shown and comprehensively characterised by FT-IR, XPS and EXAFS (for Pd adsorbed by CS,(Kramareva et al., 2004)).

3.2 Characterisation of CS-based cryogels containing PtNPs or PdNPs.

SEM images showed the macroporous structure of the CS-GA-PdNPs cryogels, which were defined by thin walls, due to utilisation of CS in diluted acetic acid (Figure 2(a,b)). Previously, the concentration effect of osmolytes on the thickness of cryogel walls has been shown (Kirsebom et al., 2013). TEM analysis was used to examine the dimensions and distributions of PdNPs and PtNPs within the cryogel (Figure 2(c,d)), with images showing the presence of well-dispersed (non-aggregated) NPs embedded in the cryogel pore walls.

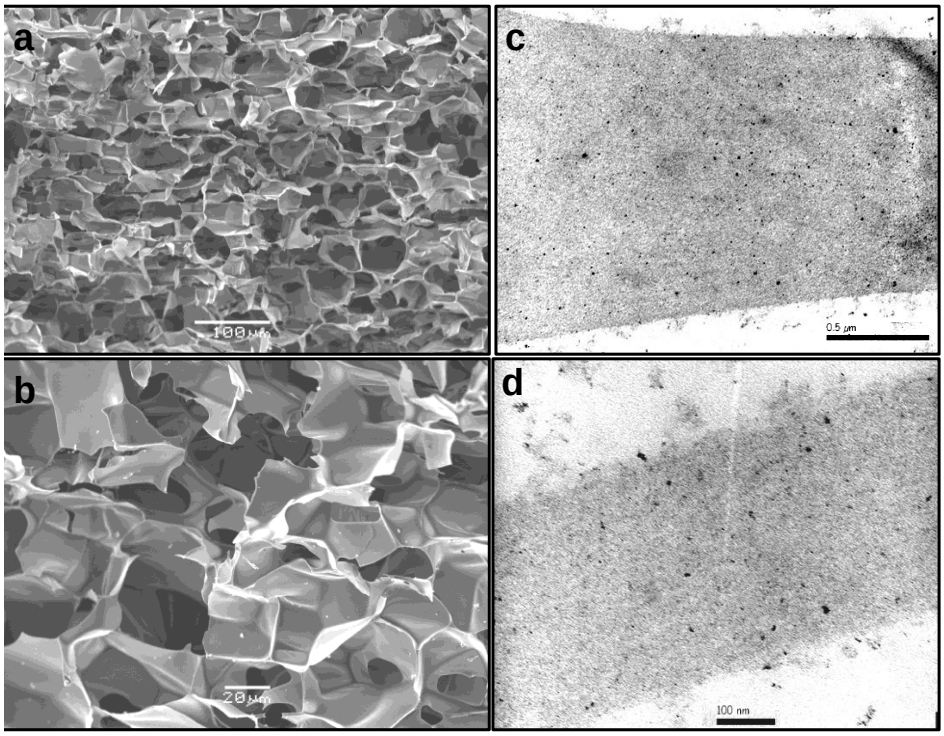

Figure 2. SEM (a, b) and TEM (c, d) images for CS-GA-PdNPs cryogel containing 0.8 mM of PdNPs at low and high magnification.

The utilisation of GA produces a chemically cross-linked dense network, which successfully prevents the subsequent aggregation of the *in-situ* formed nanoparticles. The reduction of platinum or palladium complexes in the presence of CS by sodium borohydride ($NaBH_4$) results in formation of PtNPs with a diameter in the range of 2.0 - 3.5 nm. Alteration of the ratio of palladium salt to $NaBH_4$ did not affect the size distribution of PdNPs (Adlim et al., 2004; Laudenslager et al., 2008). There are no published data on the size distribution of PtNPs or PdNPs prepared by the use of GA. The average size distributions of PdNPs and PtNPs in the cryogel walls were estimated using Image J software which indicated the presence of NPs mostly of diameter 2.4 nm and 2.2 nm, respectively (Figure 3). PdNPs and PtNPs were well distributed in the CS-GA cryogel.

As can be observed on the TEM images PdNPs were characterised by a mixed morphology, although we approximate that most of the particles had close to spherical shape, (Figure 2, 3) therefore histograms of size distributions of PdNPs and PtNPs within the cryogel walls were illustrated via comparison of the diameter of particles (Figure 3).

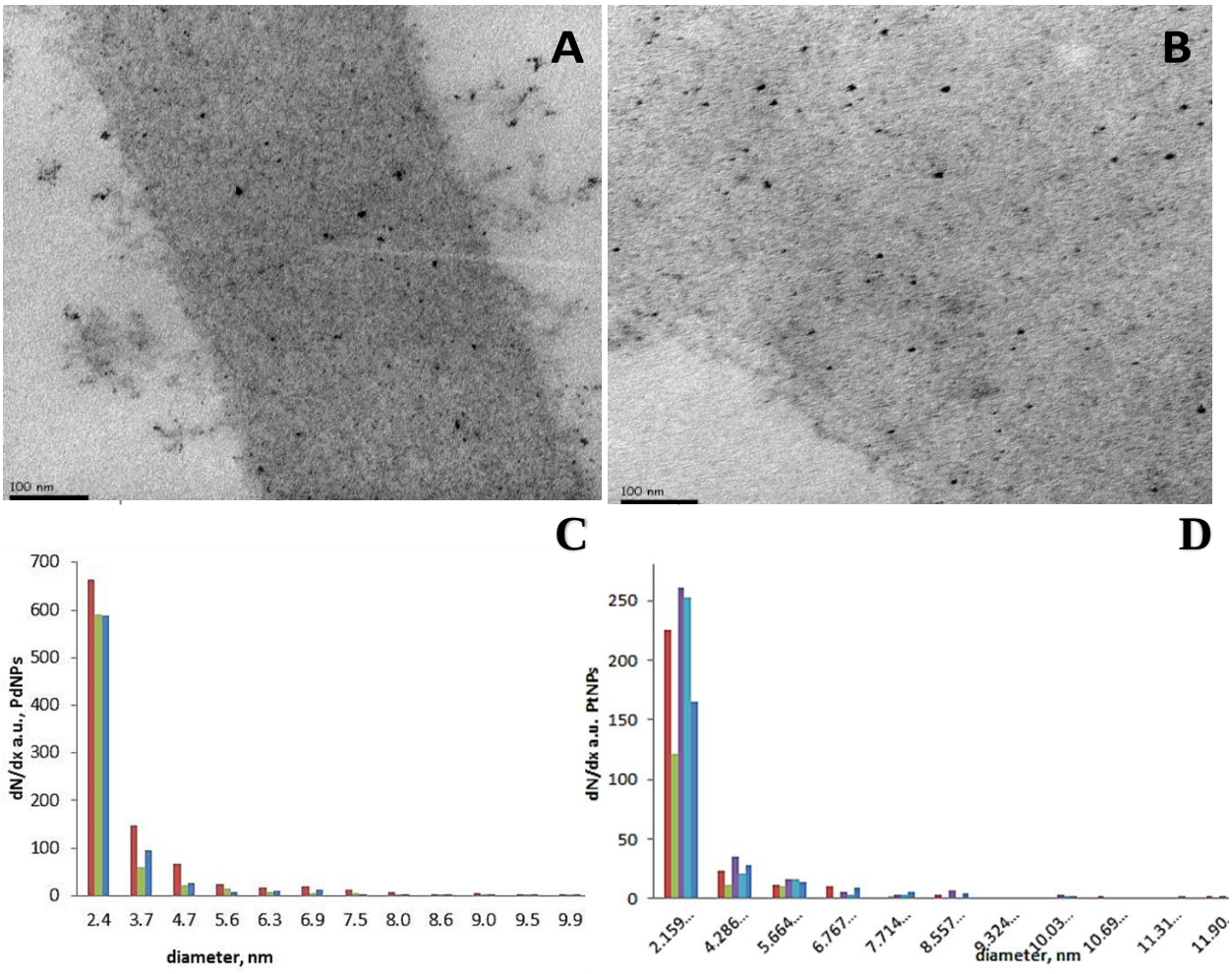

Figure 3. TEM images of cryogel walls of: A) CS-GA-PdNPs, B) CS-GA-PtNPs. Histogram of size distribution of: C) PdNPs (0.8 mM) and D) PtNPs (4 mM) in the walls of the cryogel by diameter (different colours correspond to TEM analysis of different sites within the cryogels).

The macroporous structure of the cryogels in a wet state was evaluated using LCSM microscopy (Figure 4). SEM and LCSM images of CS-GA-PdNPs revealed similar sample macroporous morphology.

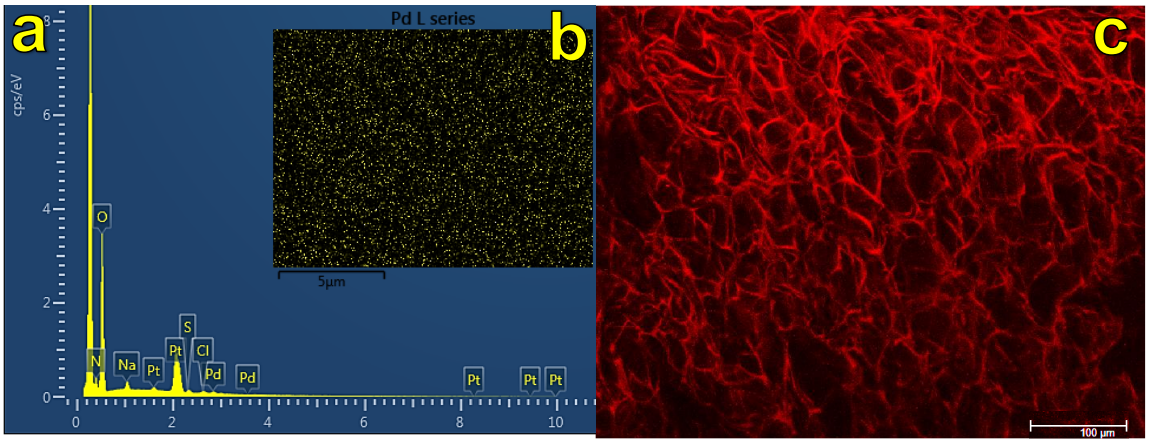

Figure 4. a) Energy-dispersive X-ray spectroscopy analysis of CS-GA-PdNPs cryogel containing 1 mM PdNPs (presence of Pt in the spectrum is due to use of platinum as a sample coating material); b) Elemental mapping for PdNPs in the walls of the cryogel (yellow colour, black colour = polymer; c) LCSM of CS-GA-PdNPs cryogel containing 0.8mM PdNPs (Pd-VI). Image C shows the macroporous structure of the cryogels composed of interconnected (open) pores - the red colour illustrates the polymer, while the black colour is attributed to pores within the cryogel (voids/ empty space).

The cryogel with *in-situ* incorporated PtNPs was also characterised by a typical macroporous structure with open pores. At least 10 TEM images were taken from different parts of the material. PtNPs were evenly distributed within the walls of the cryogel, and few aggregates of PtNPs were found (Figures 2 and 3). EDX spectroscopy confirmed the presence of noble metal within the material and elemental mapping together with TEM illustrated the dispersed nature of the nanoparticles (Figures 3&4). Imaging methods such as SEM (Figure 2) and LCSM (Figure 4) provide high resolution microphotographs of the internal structure of CS-GA-PdNPs cryogels. However, to estimate the heterogeneity in channel and pore structure a nitrogen adsorption analysis technique was used to (a) quantify the surface area of the material, and (b) examine the nanoporosity of the material. Table S1 summarises the experimental results obtained for cryogels by applying three different adsorption models (isotherms), namely BET, BJH and DFT (Figure S2-S3). The surface area (SBET) of the CS cryogel, and 0.2mM PdNPs-CS-GA and 0.4mM

PdNPs-CS-GA cryogels was 94, 24 and 43 m^2/g, respectively, which is similar to surface area measurements reported for PVA-GA cryogels (Zheng, 2013). The pore diameter of the CS cryogel, and 0.2mM PdNPs-CS-GA and 0.4mM PdNPs-CS-GA cryogels, was evaluated using the BJH model, which gave calculated (nano)pore diameters equal to 3.06, 3.83 and 3.06 nm respectively (Figure S3).

3.3 TGA analysis of cryogels with *in situ* formed PdNPs

Under TGA analysis, the cryogel CS-GA-[$PdCl_4$] showed an initial weight loss of 6-7 % before 100℃ due to loss of water adsorbed from air during storage and sample preparation. The primary degradation of pure CS started at about 234 °C, and the CS was completely degraded at 450 °C with a weight loss of 78 %. The degradation of dry hydrogel composed of CS-GA and PdNPs correlated with the degradation profile of the pure CS-GA cryogel in an atmosphere of nitrogen (Figure S4). It should be noted that there is a significant difference in the amount of solid residue after decomposition of pure CS-GA and the CS-GA-PdNPs (0.05 mM) cryogels in an atmosphere of air of 38 % and one %, respectively. One can assume that the mechanism of decomposition of the material is different, which is most probably related to the catalytic activity of PdNPs, which presumably catalyses polymer destruction during heating (Supplementary information).

3.4 Catalytic activity of cryogel-hosted PdNPs

To demonstrate the properties of the obtained macroporous cryogels in term of their application as a superior catalytic scaffold for a variety of reactions, a model system using 4-nitrophenol (4NP) was examined. Cryogels with impregnated PdNPs were here tested as catalysts for the reduction reaction of 4NP by $NaBH_4$. 4-nitrophenol (4NP) is a priority pollutant and one of the most common industrial nitroaromatic compounds, generated during a range of processes including drug (paracetamol) and pesticide manufacture, leather treatment and dyestuffs production. The reduction of 4NP to 4-aminophenol with an excess amount of $NaBH_4$ has been used by a number of authors as a model reaction to examine the catalytic performance of metal NPs (Kuroda, Ishida,

& Haruta, 2009; Menumerov, Hughes, & Neretina, 2016). The catalytic effectivity of three different quantities of PdNPs (2.66, 10.6 and 21.2 μg), supported by cryogels, under various conditions (4NP concentration, temperature) were studied in batch mode using UV-spectrophotometry. Pseudo-first order reaction rate constants (*k*) were calculated under identical reaction conditions using plots of $\ln(A_t)$ vs. time *t*, which gives a straight line with a slope of *minus*. Under UV-spec. analysis, the intensity of the absorbance of the nitro group at 400 nm decreased with time, and concurrently, a band with increased absorbance intensity appeared at 300 nm, illustrating the conversion of 4NP to the reduction product 4-aminophenol (4AP4) (Menumerov et al., 2016; Murugan & Vimala, 2013). The catalytic activity of the macroporous materials (PtNPs-CS-GA and CS-GA-PdNPs) did not reduce over multiple treatment cycles (n = 7, Figure S6, n = 10, Table 1), confirming relative stability of the catalyst and the catalytic process over time (and over at least 10 repeat cycles).

As we used much higher concentrations of sodium borohydride than of 4NP, it can be assumed that the former remains basically invariable during the reaction. Under these conditions, the pseudo-first-order reaction kinetics of the reduction of 4NP can be utilised to estimate the catalytic rate. A linear correlation with time, that is, $\ln(A_t/A_0)$ (where A_t stands for absorbance at 400 nm at time t and A_0 stands for absorbance at 400 nm at time 0) versus time plot, was observed. The value of the pseudo-first-order reaction rate constant (k, determined from linear fitting) is presented in Tables 1-3 and Figure 5. Calculation of the kinetic rate was performed for the linear region of the kinetic curve for 90 minutes. The conversion degree of 4NP by 21.2 μg of PdNPs at the 10^{th} catalytic cycle was 85-96 % (Table 1).

Conversion degree data of 4NP using 11μg of PdNPs in Pd-XI cryogels revealed reproducible results, with a conversion of about 60-75 % over 50 minutes (Table 3).

Comparison of the conversion degrees of 4NP using PdNPs (10.6 μg) between Pd-XI and Pd-IV cryogels did not show significant differences for periods of time of up to 50 minutes (Figure S7i,ii). However, TON and TOF parameters for Pd-IV cryogels were higher compared to Pd-XI samples (Table 2). The control sample (CS-GA cryogels) showed some adsorption of 4NP (Figure S8i),

but control experiments showed that reduction of 4NP in the presence of $NaBH_4$, but without noble metal nanoparticles, did not occur (Figure S8ii).

Table 1. Rate constants of 4NP reduction catalysed by Pd-V cryogel and degree of conversion (DC) at time points 60 and 120 min, at different reaction temperatures. The concentration of sodium borohydride[H] was 22.2 mmol L^{-1} unless otherwise specified. Conditions were:a) [4NP] 3.8 µM, V 3.5 mL, b) [4NP] 2.1 µM , V 7 mL.

a, **22 ℃**				b, **22 ℃**		b, **35 ℃**			b, **10 ℃**	
Catalytic cycle number	DC_{120}, %	k *10^{-3}, min^{-1}	[H] mmol L^{-1}	DC_{120}, %	k *10^{-3}, min^{-1}	$DC_{60\ min}$, %	$DC_{120\ min}$, %	k *10^{-3}, min^{-1}	DC_{120}, %	k *10^{-3}, min^{-1}
1	77.5	15.2	8.7	63.1	8.1	62.4	81	14.1	50.38	6.8
2	86.4	18.7	8.7	78.6	11.8	66.5		18.7	54.1	8.1
3	91	22.2	16.5	77.5	13.5	71.2	88.4	19.5	61.22	8.2
4	91	23.0	17.4	85.34	17.2				69.13	9.4
5	93	24.1	22.2	67.92x	10.4					
x6	85.4	19.3	22.2	77.7	12.9					
7	98	37.4	22.2	65.6x	12.1					
8	98.9	39.8	22.2	78	13.7					
9	96.2	34.5	22.2	81.9	15.8					
10	96.4	30.9	22.2	85	17.9					

x experiment continued on the next day (overnight break between cycles).

A two times dilution of 4NP, but keeping the amount of the substrate (umol:umol) comparable in both cases (comparable to increasing the volume) led to a decrease of 4NP conversion at 22 °C of

approximately 10 % (Table 1), which is most probably related to diffusion limitation due to the dilution effect, which in turn is in agreement with a decrease of the kinetic rate by 55-60%. It was observed that the kinetic rate for the first catalytic cycle at different temperatures was in the range of 20-40% less compared to the following cycles, which is related to a certain activation time needed to saturate PdNPs with hydrogen within the cryogel (Table 1). An increase of sodium borohydride concentration from 8.7 mM to 16.5 and 22.2 mM for the same volume and concentration of 4NP resulted in an increase of the rate at room temperature by (on average) 33 and 82 %, respectively (Table 1(a), Figure 5a (PdV)). It is noteworthy that if the next experimental cycle continued after an overnight break or on a subsequent day, the degree of conversion decreased by approximately 10% compared to the following catalytic reaction performed, this as noted previously is related to the saturation of the PdNPs with a sufficient amount of hydrogen (Figure 5). It is important to note that the conversion of 4NP did not decline over 10 cycles (Figure S8), showing a conversion degree of 96 % for the sample containing 21 μg PdNPs for Pd-V (Figure 5a). Increasing the temperature of the catalytic reaction from 10 to 22 and 35°C by Pd-V increased the kinetic rate by 1.44 and 2.26 times, respectively (Table 1(b) and Figure 5c).

Apparent TON and TOF for the catalyst PdNPs (21 μg) for 10 catalytic cycles were 6.03 and 0.3 h^{-1}, respectively (Table 2). The TOF parameter clearly illustrates an enhancement in catalytic efficiency for the reduction reaction with an increase of temperature, i.e. TOF at 10, 22 and 35°C was 0.1, 0.3 and 0.38h^{-1}, respectively (Table 2). Catalytic reduction of 4-NP by commercial Pd/C shows a TOF value of about 0.36 s^{-1} and TOF of Pd@MIL-100(Fe) was 0.50 s^{-1}(Xu, Li, Chen, Zhang, & Li, 2018). The reported TON and TOF are not the final data because decline of the catalytic activity was not observed over the course of the experiment (Table 1, b), and typically the final values of the TON and TOF parameters are obtained when the catalyst has lost its catalytic activity.

Table 2. TON and TOF parameters of immobilised PdNPs catalyst for reduction of 4NP. Superscript numbers on TON & TOF data were calculated for: a & c)7 cycles; b) 13 cycles; d) 10 cycles; e) 4 cycles; f) 3 cycles, g) 9 cycles.

Sample name	V 0.5 mL, [PdNPs], mM	M (PdNPs), µg	Sample	total time of catalytic reactions, h	[4NP], µmol	TON	TOF, h^{-1}
Pd-X	0.05	2.8	a	14.26	0.10	3.833[a]	0.268
Pd-X	0.05	2.66	b	19.36	0.256	10.245[g]	0.529
Pd-X	0.05	2.66	b	15.3	0.198	7.925 [a]	0.518
Pd-IV	0.2	12.5	a	9.8	0.287	2.44[a]	0.249
Pd-IV	0.2	12.5	a	18.95	0.542	3.95[b]	0.208
Pd-IV	0.2	13.3	b	9.22	0.286	2.298[a]	0.249
Pd-IV	0.2	13.3	b	21.0	0.463	4.34[b]	0.206
Pd-XI	0.2	11.2	a, ACN	15.62	0.322	2.98[c]	0.19
Pd-XI	0.2	12	b, ACN	16.1	0.313	2.86[c]	0.178
Pd-V	0.4	21	a, T 22 °C	20.1	1.20	6.03 [d]	0.30
Pd-V	0.4	21	b, T 22 °C	21.86	1.245	6.23[d]	0.285
Pd-V	0.4	21	b, T 10 °C	7.78	0.179	0.899[e]	0.10
Pd-V	0.4	21	b, T 35 °C	5.0	0.38	1.89[f]	0.38

Comparison of TON and TOF parameters for different amounts of immobilised catalyst indicates that Pd-X provided the highest values for TON and TOF (Table 2), however this case has a relatively low conversion degree (Table S2). Such a material can still be suggested for environmental application, however, where the contact time (particularly in batch treatment mode) can be prolonged. Concurrently, Pd-V revealed a conversion degree of 4NP to 4AP up to 98.9 % with a reasonably high TON of 0.38 h^{-1}, and may be suggested for industrial catalytic use (Tables

1-2). Calculations of the kinetic rate were performed for the linear region of the kinetic curve for 90 minutes (Table 3). An increase in the reaction time from 80 to 120 min did not significantly increase the conversion of 4NP, therefore there are limited benefits for prolonging solution exposure time to the catalyst – instead relatively short treatment times can be used before passing on process wastes to following separation or adsorption steps. If considering the use of the supported catalyst for environmental applications, the catalytic system could be used to reduce 4NP concentrations by 85-95%, following which trace amounts of the contaminant might be removed by subsequent adsorbents.

Figure 5. Conversion degree of 4AP: a) 120 min; b) 80 min; c) different temperatures (10, 22 and 35°C) for120 min. Calculated under following parameters: 0.67 μM [4NP], V 7mL for cryogels Pd-XI and Pd-IV; 1.3 μM [4NP], V 7 mL for cryogels Pd-IV*; a, [4NP] 3.8 μM, V 3.5 mL and b, V 7 mL, [4NP] 2.1 μM, for cryogels Pd-V.

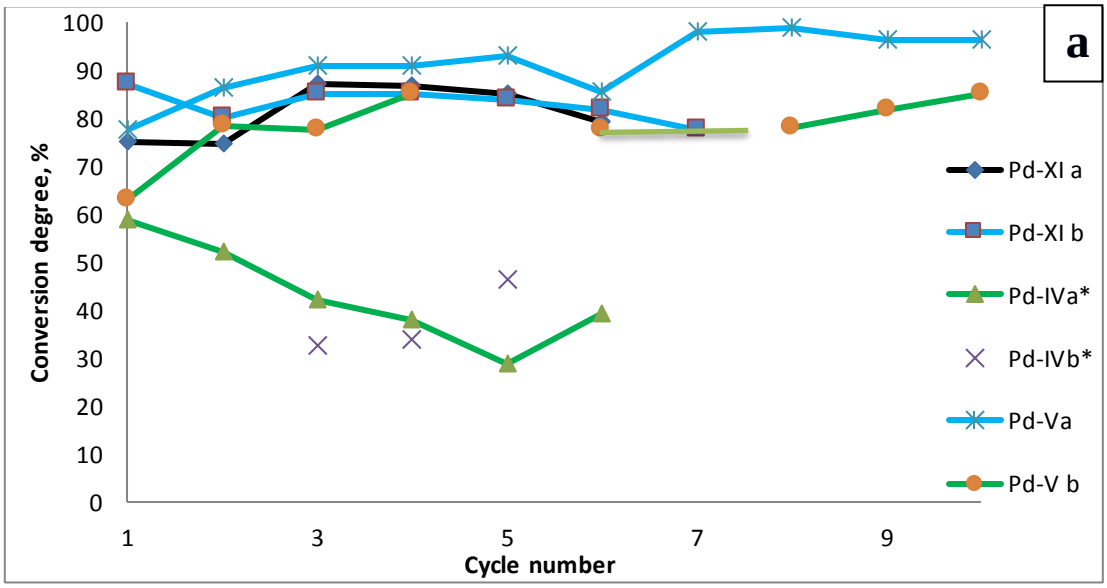
a
Conversion degree, %
Cycle number
Pd-XI a
Pd-XI b
Pd-IVa*
Pd-IVb*
Pd-Va
Pd-V b

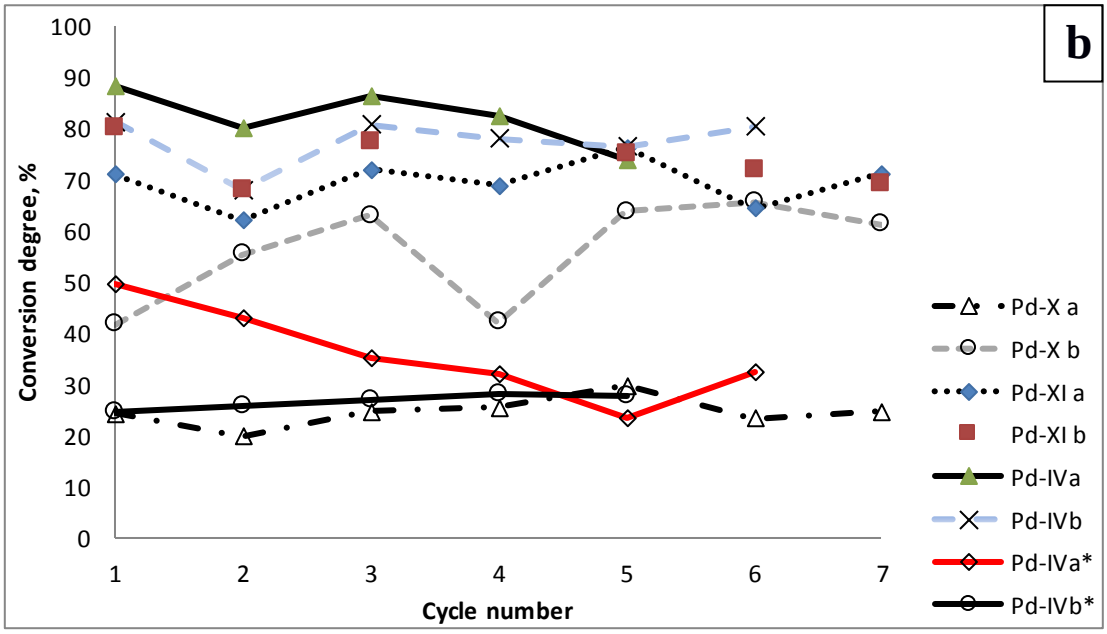
b
Conversion degree, %
Cycle number
Pd-X a
Pd-X b
Pd-XI a
Pd-XI b
Pd-IVa
Pd-IVb
Pd-IVa*
Pd-IVb*

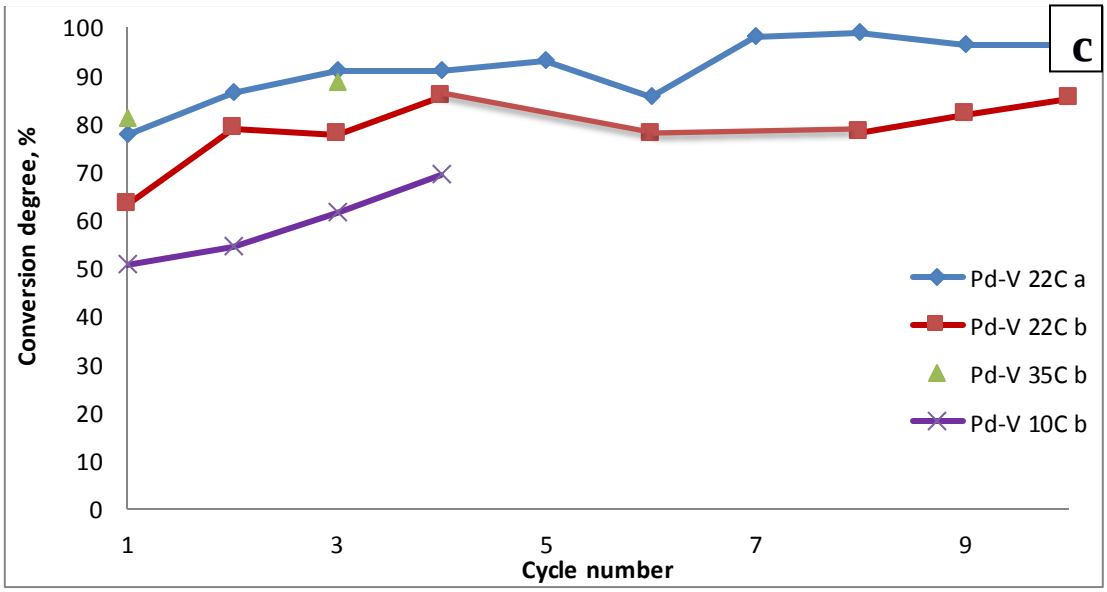
c
Conversion degree, %
Cycle number
Pd-V 22C a
Pd-V 22C b
Pd-V 35C b
Pd-V 10C b

Table 3. Rate constants and conversion degree of 4AP. Kinetic rates were calculated for the linear region of the kinetic curves over 80 minutes at the following conditions: 0.67 uM of 4NP, V 7mL for cryogels Pd-XI and Pd-IV; 1.3 μM of 4NP, 7 mL for cryogels Pd-IVi.

cycle number	$DC_{120\ min}$ Pd-XI, %	$k_{Pd\text{-}XI}$ $*10^{-3}$ (a), min^{-1}	$k_{Pd\text{-}XI}$ $*10^{-3}$ (b), min^{-1}	DC_{80min} Pd-IV, %	$k_{Pd\text{-}IV}$ $*10^{-3}$ (a) min^{-1}	$k_{Pd\text{-}IV}$ $*10^{-3}$ (b) min^{-1}	$DC_{120\ min\ Pd\text{-}IV^*}$, %	$k_{Pd\text{-}IV^*}$ $*10^{-3}$ (a) min^{-1}	$k_{Pd\text{-}IV^*}$ $*10^{-3}$, (b) min^{-1}
1	81.3 ± 8.4	19.7	14	84.2 ±5.9	22.8	21.1	24.6	7.4	5.2
2	77.4 ± 3.6	13.5	12.2	74.0±8.4	19.2	13.8	25.85	6.6	4.4
3	86.3 ±1.5	17.1	14.4	83.45± 3.9	29	21.6	37.2 ± 6.8	5.1	4.2
4	85.8 ± 1.13	16.4	18.5	80.1±3.0	29.3	20.2	35.85 ± 3.04	3.2	4.1
5	84.5 ± 0.7	16.6	17	75.1±1.8	27.4	19	37.6 ± 12.1	3.0	4.6
x6	80.65 ±1.9	14.8	13	80.4±2.0	29.1	19	39.3	4.5	
7	77.8±1.2	13.9	15.6	65.0xx	31.1	17.7			

x experiment continued on the next day(overnight break at 4°C between cycles).

xx 60 minutes

A comparison of the conversion degree and kinetic constants for samples containing the same amount of Pd catalyst (Pd-IV and Pd-XI), but prepared in the presence of and without acetonitrile (ACN) is given in Table 3 and Figure 5a&b. The supported catalysts prepared in the presence of

acetonitrile illustrated an average rate for seven cycles of 15.9±2.1 min^{-1} , lower than the rate for samples prepared without acetonitrile (22.9±5.3 min^{-1}), which might be related to some loss of Pd catalyst during the cryogel preparation procedure (as the introduced acetonitrile may inhibit rapid ligand exchange with CS and therefore some amounts of the Pd complex may not bind to CS, which is in agreement with viscosity data (Figure S1)).

Doubling the 4NP concentration while keeping the the same volume of the reaction mixture led to a halving of the conversion degree for the same period of time for cryogels Pd-IV and Pd-IV* (Table 3). Data for kinetic rates (Tables 1 & 3, A2) illustrate that palladium nanoparticles (Pd-IV, V, X and XI) can be reused over a number of treatment cycles (Tables 1 & 3, A4). Every sample was tested from 4 to 17 cycles for the catalytic reduction of 4NP (2 - 3.5 µM) by $NaBH_4$ at 22 °C. It was observed that the activity showed no significant decrease after reuse for 17 cycles. This indicated that the PdNPs were not deactivated, or washed out or poisoned, during the catalytic process (Figure 5a).

The observed rates of catalytic reduction using PdNPs correlate well with those reported in the literature, for example, rates using a polyanilin-PdNPs composite (bulk) with a (Pd) weight of 130, 390 and 650 µg were $4.8*10^{-3}$, $11*10^{-3}$ $17.7*10^{-3}$ $mol^{-1}min^{-1}$ (Komathi et al., 2010). In this study however 30 - 40 times less palladium catalyst was used. The same reaction catalysed by a hybrid of multi-walled carbon nanotubes and an amphiphilic poly-(propyleneimine) dendrimer immobilised with PdNPs demonstrated a constant rate of $14.6*10^{-3}$ min^{-1} (Murugan & Vimala, 2013). Esumi et al., (2004) reported that the *k* for PdNPs catalysts supported on multi-walled carbon nanotubes was equal to $2.958*10^{-3}$ min^{-1}.The comparison of kinetic rates with other previously published Pd catalyst data for nitrophenol reduction is presented in Table S3. The main advantages of the present system compared to other PdNPs catalyst systems are the absence of a separation step for the PdNPs, and the use of (a) a two-step preparation method, (b) a significantly lower amount of the catalyst (3-21 µg Pd), and (c) relatively inexpensive chemical precursors (in the case of chitosan, based on a naturally-derived and common biopolymer). Macroporous cryogel scaffolds have been shown to be capable of production in a variety of shapes and configurations

and the cryogel production process can also be readily scalable to much larger scaffold/sample volumes (Savina et al., 2016), giving high potential for practical engineering / environmental application.

Conclusion

In this paper, we have illustrated a two-step preparation procedure for mechanically stable macroporous materials with incorporated noble metal nanoparticles. The cryogelation of CS with Pd complexes led to 99.66 % noble metal binding due to cryoconcentration effects and ligand exchange processes. The following freeze drying step helps to achieve nearly 100% metal binding. Using a complex of tetrachloropalladate in the presence of acetonitrile it is possible to prepare a catalyst with higher metal content and to delay hydrogel formation, which was confirmed by a slowed increase in the viscosity of the CS solution. *In situ* preparation of Pt and Pd nanoparticles incorporated into the cryogel walls using glutaraldehyde as a reducing (and cross-linking) agent was proposed. The absence of leakage of noble metal complexes and nanoparticles from the macroporous scaffolds was confirmed using ICP-MS. The catalytic activity of the macroporous material was evaluated using a model reaction of 4NP reduction by sodium borohydride. It was observed for all experiments that the initial conversion degree of 4NP was 10% less on the first cycle compared to the following catalytic cycles, which is attributed to a certain time needed to saturate PdNPs with hydrogen. Increasing the temperature of the catalytic reaction from 10 to 22 and 35°C by PdNPs supported within the cryogel increased the kinetic rate by 1.44 and 2.26 times, respectively. PdNPs prepared in the presence of acetonitrile illustrated an average rate for seven cycles of 15.9 ± 2.1 min^{-1}, lower than the rate for cryogels prepared without acetonitrile (22.9 ± 5.3 min^{-1}). TON and TOF parameters for four types of PdNPs supported cryogels were calculated for 10 catalytic cycles. TON and TOF for the macroporous materials with 2.66 μg 13.3 μg and 21 μg of incorporated PdNPs were 10.24 & 0.529 h^{-1}; 4.34 & 0.206 h^{-1}; 6.22 & 0.285 h^{-1}, respectively. The conversion degree of 4NP for a catalyst content of 21 μg of PdNPs reached 98.9 % at room temperature. The catalytic activity for 4NP conversion did not decline significantly over the testing

period. Significantly less weight of palladium nanoparticles (30-40 times) was needed compared to published data to obtain comparable kinetic rates of reduction of 4-nitrophenol.

Conflict of Interest Disclosure

Authors declare no competing financial interest.

Acknowledgements

DB gratefully acknowledges the European Union's Horizon 2020 research and innovation programme under the Marie Skłodowska-Curie Fellowship grant agreement N 701289, which supported his time when writing this paper. The authors are grateful to the Department of Biotechnology and personally Emeritus Prof. Bo Mattiasson of Lund University for providing access to facilities and chemicals. The authors also acknowledge Dr. Yishan Zheng from University of Brighton for assistance with nitrogen adsorption experiments and Mr Peter Lyons from the School of Environment and Technology at the University of Brighton for help with analysis of samples using ICP-MS.

REFERENCES:

Adlim, M., Abu Bakar, M., Liew, K. Y., & Ismail, J. (2004). Synthesis of chitosan-stabilized platinum and palladium nanoparticles and their hydrogenation activity. *Journal of Molecular Catalysis A: Chemical,* 212(1–2), 141-149.

Ali, M. E., El-Aty, A. M. A., Badawy, M. I., & Ali, R. K. (2018). Removal of pharmaceutical pollutants from synthetic wastewater using chemically modified biomass of green alga Scenedesmus obliquus. *Ecotoxicology and environmental safety,* 151, 144-152.

Berger, J., Reist, M., Mayer, J. M., Felt, O., Peppas, N., & Gurny, R. (2004). Structure and interactions in covalently and ionically crosslinked chitosan hydrogels for biomedical applications. *European Journal of Pharmaceutics and Biopharmaceutics,* 57(1), 19-34.

Berillo, D., Mattiasson, B., & Kirsebom, H. (2014). Cryogelation of Chitosan Using Noble-Metal Ions: In Situ Formation of Nanoparticles. *Biomacromolecules,* 15(6), 2246-2255.

Berillo, D., & Volkova, N. (2014). Preparation and physicochemical characteristics of cryogel based on gelatin and oxidised dextran. *Journal of Materials Science,* 49(14), 4855-4868.

Bertoni, F. A., González, J. C., García, S. I., Sala, L. F., & Bellú, S. E. (2018). Application of chitosan in removal of molybdate ions from contaminated water and groundwater. *Carbohydrate polymers,* 180, 55-62.

Boufi, S., Vilar, M. R., Ferraria, A. M., & do Rego, A. M. B. (2013). In situ photochemical generation of silver and gold nanoparticles on chitosan. *Colloids and Surfaces A: Physicochemical and Engineering Aspects,* 439, 151-158.

Brack, H., Tirmizi, S., & Risen, W. (1997). A spectroscopic and viscometric study of the metal ion-induced gelation of the biopolymer chitosan. *Polymer*, 38(10), 2351-2362.

Bronstein, L., Sidorov, S., Gourkova, A., Valetsky, P., Hartmann, J., Breulmann, M., . . . Antonietti, M. (1998). Interaction of metal compounds with 'double-hydrophilic'block copolymers in aqueous medium and metal colloid formation. *Inorganica Chimica Acta*, 280(1-2), 348-354.

Corma, A., & Garcia, H. (2008). Supported gold nanoparticles as catalysts for organic reactions. *Chemical Society Reviews*, 37(9), 2096-2126.

Dainiak, M. B., Allan, I. U., Savina, I. N., Cornelio, L., James, E. S., James, S. L., . . . Galaev, I. Y. (2010). Gelatin–fibrinogen cryogel dermal matrices for wound repair: preparation, optimisation and in vitro study. *Biomaterials*, 31(1), 67-76.

Draget, K. I., Värum, K. M., Moen, E., Gynnild, H., & Smidsrød, O. (1992). Chitosan cross-linked with Mo (VI) polyoxyanions: a new gelling system. *Biomaterials*, 13(9), 635-638.

El Kadib, A. (2015). Chitosan as a sustainable organocatalyst: a concise overview. *ChemSusChem*, 8(2), 217-244.

Emin, C., Gu, Y., Remigy, J.-C., & Lahitte, J.-F. (2015). Polyethersulfone hollow fiber modified with poly (styrenesulfonate) and Pd nanoparticles for catalytic reaction. *The European Physical Journal Special Topics*, 224(9), 1843-1848.

Guibal, E. (2005). Heterogeneous catalysis on chitosan-based materials: a review. *Progress in Polymer Science*, 30(1), 71-109.

Guibal, E., Sweeney, N. V. O., Vincent, T., & Tobin, J. (2002). Sulfur derivatives of chitosan for palladium sorption. *Reactive and Functional Polymers*, 50(2), 149-163.

Gun'ko, V. M., Savina, I. N., & Mikhalovsky, S. V. (2013). Cryogels: morphological, structural and adsorption characterisation. *Advances in colloid and interface science*, 187, 1-46.

Hagen, J. (2015). *Industrial catalysis: a practical approach*: John Wiley & Sons.

Hataf, N., Ghadir, P., & Ranjbar, N. (2018). Investigation of soil stabilization using chitosan biopolymer. *Journal of Cleaner Production*, 170, 1493-1500.

Hu, S., Bi, S., Yan, D., Zhou, Z., Sun, G., Cheng, X., & Chen, X. (2018). Preparation of composite hydroxybutyl chitosan sponge and its role in promoting wound healing. *Carbohydrate polymers*, 184, 154-163.

Kasaai, M. R. (2010). Determination of the degree of N-acetylation for chitin and chitosan by various NMR spectroscopy techniques: A review. *Carbohydrate polymers*, 79(4), 801-810.

Kirsebom, H., Elowsson, L., Berillo, D., Cozzi, S., Inci, I., Piskin, E., . . . Mattiasson, B. (2013). Enzyme-Catalyzed Crosslinking in a Partly Frozen State: A New Way to Produce Supermacroporous Protein Structures. *Macromolecular bioscience*, 13(1), 67-76.

Komathi, S., Palaniappan, S., Manisankar, P., Gopalan, A. I., & Lee, K. P. (2010). Large Scale Preparation of Palladium Nanoparticles Loaded Polyaniline Nanostructures through Seed Induced Bulk Polymerization. *Macromolecular Chemistry and Physics*, 211(12), 1330-1338.

Kramareva, N. V., Stakheev, A. Y., Tkachenko, O. P., Klementiev, K. V., Grünert, W., Finashina, E. D., & Kustov, L. M. (2004). Heterogenized palladium chitosan complexes as potential catalysts in oxidation reactions: study of the structure. *Journal of Molecular Catalysis A: Chemical*, 209(1), 97-106.

Kurita, K. (2006). Chitin and chitosan: functional biopolymers from marine crustaceans. *Marine Biotechnology*, 8(3), 203-226.

Kuroda, K., Ishida, T., & Haruta, M. (2009). Reduction of 4-nitrophenol to 4-aminophenol over Au nanoparticles deposited on PMMA. *Journal of Molecular Catalysis A: Chemical*, 298(1), 7-11.

Laudenslager, M. J., Schiffman, J. D., & Schauer, C. L. (2008). Carboxymethyl chitosan as a matrix material for platinum, gold, and silver nanoparticles. *Biomacromolecules*, 9(10), 2682-2685.

Li, Y., Wu, Y., Xu, Q., Gao, Y., Cao, G., Meng, Z., & Yang, C. (2013). Facile and controllable synthesis of polystyrene/palladium nanoparticle@ polypyrrole nanocomposite particles. *Polymer Chemistry*, 4(17), 4655-4662.

Liu, X., Ruiz, J., & Astruc, D. (2017). Compared Catalytic Efficiency of Click-Dendrimer-Stabilized Late Transition Metal Nanoparticles in 4-Nitrophenol Reduction. *Journal of Inorganic and Organometallic Polymers and Materials*, 1-8.

Loo, S.-L., Krantz, W. B., Fane, A. G., Hu, X., & Lim, T.-T. (2015). Effect of synthesis routes on the properties and bactericidal activity of cryogels incorporated with silver nanoparticles. *RSC Advances*, 5(55), 44626-44635.

Lozinsky, V., Zubov, A., Kulakova, V., Titova, E., & Rogozhin, S. (1992). Study of cryostructurization of polymer systems. IX. Poly (vinyl alcohol) cryogels filled with particles of crosslinked dextran gel. *Journal of applied polymer science*, 44(8), 1423-1435.

Lozinsky, V. I., Galaev, I. Y., Plieva, F. M., Savina, I. N., Jungvid, H., & Mattiasson, B. (2003). Polymeric cryogels as promising materials of biotechnological interest. *TRENDS in Biotechnology*, 21(10), 445-451.

Lozinsky, V. I., Plieva, F. M., Galaev, I. Y., & Mattiasson, B. (2001). The potential of polymeric cryogels in bioseparation. *Bioseparation*, 10(4-5), 163-188.

Mahé, O., Brière, J. F., & Dez, I. (2015). Chitosan: An upgraded polysaccharide waste for organocatalysis. *European Journal of Organic Chemistry*, 2015(12), 2559-2578.

Maritz, B., & van Eldik, R. (1976). Kinetics and mechanism of the reduction of tetrachloroaurate (III) by malonate in acidic aqueous solution. *Inorganica Chimica Acta*, 20, 43-47.

Menumerov, E., Hughes, R. A., & Neretina, S. (2016). Catalytic Reduction of 4-Nitrophenol: A Quantitative Assessment of the Role of Dissolved Oxygen in Determining the Induction Time. *Nano letters*, 16(12), 7791-7797.

Murugan, E., & Vimala, G. (2013). Synthesis, characterization, and catalytic activity for hybrids of multi-walled carbon nanotube and amphiphilic poly (propyleneimine) dendrimer immobilized with silver and palladium nanoparticle. *Journal of colloid and interface science*, 396, 101-111.

Oelschlaeger, C., Bossler, F., & Willenbacher, N. (2016). Synthesis, Structural and Micromechanical Properties of 3D Hyaluronic Acid-Based Cryogel Scaffolds. *Biomacromolecules*, 17(2), 580-589.

Qu, X., Wirsén, A., & Albertsson, A. C. (1999). Structural change and swelling mechanism of pH-sensitive hydrogels based on chitosan and D, L-lactic acid. *Journal of applied polymer science*, 74(13), 3186-3192.

Qu, X., Wirsén, A., Olander, B., & Albertsson, A.-C. (2001). Surface modification of high density polyethylene tubes by coating chitosan, chitosan hydrogel and heparin. *Polymer Bulletin*, 46(2), 223-229.

Sachse, A., Galarneau, A., Fajula, F., Di Renzo, F., Creux, P., & Coq, B. (2011). Functional silica monoliths with hierarchical uniform porosity as continuous flow catalytic reactors. *Microporous and Mesoporous Materials*, 140(1), 58-68.

Savina, I. N., Ingavle, G. C., Cundy, A. B., & Mikhalovsky, S. V. (2016). A simple method for the production of large volume 3D macroporous hydrogels for advanced biotechnological, medical and environmental applications. *Scientific reports*, 6.

Shi, B., Zhang, H., Shen, Z., Bi, J., & Dai, S. (2013). Developing a chitosan supported imidazole Schiff-base for high-efficiency gene delivery. *Polymer Chemistry*, 4(3), 840-850.

Venkatesham, M., Ayodhya, D., & Veerabhadram, G. (2015). Green synthesis, characterization and catalytic activity of palladium nanoparticles by xanthan gum. *Applied Nanoscience*, 5(3), 315-320.

Vilian, A. E., Choe, S. R., Giribabu, K., Jang, S.-C., Roh, C., Huh, Y. S., & Han, Y.-K. (2017). Pd nanospheres decorated reduced graphene oxide with multi-functions: Highly efficient catalytic reduction and ultrasensitive sensing of hazardous 4-nitrophenol pollutant. *Journal of hazardous materials*, 333, 54-62.

Wu, Z., & Jin, R. (2010). On the ligand's role in the fluorescence of gold nanoclusters. *Nano letters*, 10(7), 2568-2573.

Xu, B., Li, X., Chen, Z., Zhang, T., & Li, C. (2018). Pd@MIL-100(Fe) composite nanoparticles as efficient catalyst for reduction of 2/3/4-nitrophenol: Synergistic effect between Pd and MIL-100(Fe). *Microporous and Mesoporous Materials*, 255(Supplement C), 1-6.

Yang, C.-H., Wang, C.-Y., Huang, K.-S., Yeh, C.-S., Wang, A. H.-J., Wang, W.-T., & Lin, M.-Y. (2012). Facile synthesis of radial-like macroporous superparamagnetic chitosan spheres with in-situ co-precipitation and gelation of ferro-gels. *PloS one*, 7(11), e49329.

Zahir-Jouzdani, F., Mahbod, M., Soleimani, M., Vakhshiteh, F., Arefian, E., Shahosseini, S., . . . Atyabi, F. (2018). Chitosan and thiolated chitosan: Novel therapeutic approach for preventing corneal haze after chemical injuries. *Carbohydrate polymers*, 179, 42-49.

Zheng, Y. (2013). Activated carbon & carbon-cryogel composites for haemoperfusion based applications. University of Brighton.